

Wall-Proximity Matters: Understanding the Effect of Device Placement with Respect to the Wall for Indoor Wireless Sensing

He Wang, *Student Member, IEEE*, Yunpeng Ge, *Student Member, IEEE*,
and Ivan Wang-Hei Ho, *Senior Member, IEEE*

Abstract—Wi-Fi sensing has been extensively explored for various applications, including vital sign monitoring, human activity recognition, indoor localization, and tracking. However, practical implementation in real-world scenarios is hindered by unstable sensing performance and limited knowledge of wireless sensing coverage. While previous works have aimed to address these challenges, they have overlooked the impact of walls on sensing capabilities in indoor environments. To fill this gap, we present a theoretical model that accounts for the effect of wall-device distance on sensing coverage. By incorporating both the wall-reflected path and the line-of-sight (LoS) path, we develop a comprehensive sensing coverage model tailored for indoor environments. This model demonstrates that strategically deploying the transmitter and receiver in proximity to the wall within a specific range can significantly expand sensing coverage. We assess the properties of our model through experiments in respiratory monitoring and stationary crowd counting applications, showcasing a notable 11.2% improvement in counting accuracy. These findings pave the way for optimized deployment strategies in Wi-Fi sensing, facilitating more effective and accurate sensing solutions across various applications.

Index Terms—Wi-Fi sensing, channel state information (CSI), sensing coverage model, device placement, wall reflection.

I. INTRODUCTION

The extensive utilization of Wi-Fi for data communication in public areas has paved the way for a remarkable discovery in recent years—the untapped potential of Wi-Fi signals for sensing applications. Leveraging channel state information (CSI) to characterize the frequency response of wireless channels in Wi-Fi systems, researchers have unlocked new avenues for sensing capabilities [1], [2]. In indoor environments, Wi-Fi signals encounter reflections from a multitude of objects, including walls and human bodies, resulting in complex multipath propagation. The variations in CSI values predominantly arise from the dynamic movements of humans. By leveraging time-frequency domain analysis, significant features can be extracted from CSI, enabling a diverse range of applications. Experimentally, CSI-based sensing has demonstrated remarkable capabilities in areas such as human activity recognition [3], [4], respiration monitoring [5], [6], crowd counting [7],

[8], and indoor positioning [9], [10]. However, it is important to note that these applications have primarily been evaluated in controlled laboratory settings with carefully designed scenarios, and their real-life applicability and scalability are yet to be fully explored.

The real-world implementation of various applications in wireless systems has been limited due to several constraints. One major limitation is the instability of sensing performance, where CSI is highly susceptible to environmental factors such as interference and configurations [11], [12]. Consequently, changes in these factors have a direct impact on the accuracy performance, particularly in deep-learning-based sensing systems. Another limitation is the restricted sensing coverage of CSI-based applications. Despite Wi-Fi signals being capable of spanning significant distances, the accurate detection range is limited to just a few meters [13]. This limitation hampers the expansion of CSI-based applications into larger spaces and more complex scenarios. However, both limitations can be mitigated through a common solution: obtaining high-quality data. By employing reliable and precise data, the instability of sensing performance can be minimized, while also enabling the extension of sensing coverage.

How to obtain high-quality data in sensing systems? Besides employing dedicated signal processing schemes [13]–[15], we may still need to go back to the fundamental knowledge regarding the sensing coverage with respect to the locations of the transceivers. The placement of sensors and the design of the sensing network play a crucial role in the quality of collected data. The sensing coverage can be expanded by changing the locations of sensors [16]. Therefore, careful consideration of factors such as sensor placement and network design becomes crucial for optimizing data collection and reducing the overall training effort. By strategically deploying devices in the sensing area, we can enhance the quality of data and overcome the limitations associated with unstable sensing performance and limited sensing coverage.

In prior research, the placement matters of wireless sensing have been investigated, leading to the observation that the sensing coverage is influenced by the distance between the transmitter (Tx) and receiver (Rx) [17]. However, this work primarily focuses on the impact of multipath on static paths and overlooks the influence of walls on dynamic paths in indoor environments. Another model addressing sensing coverage takes into account the beneficial effect of walls on through-wall sensing [18]. Nonetheless, this approach only

This work was supported in part by the Smart Traffic Fund (Project No. PSRI/31/2202/PR) established under the Transport Department of the Hong Kong Special Administrative Region (HKSAR), China.

The authors are with the Department of Electrical and Electronic Engineering, The Hong Kong Polytechnic University, Hong Kong, SAR, China (e-mail: edana.wang@connect.polyu.hk; yunpeng.ge@connect.polyu.hk; ivanwh.ho@polyu.edu.hk).

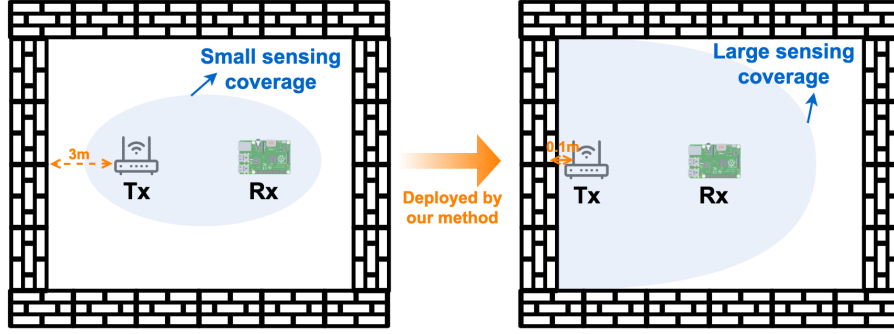


Fig. 1. Enhancing sensing coverage through device deployment.

considers scenarios where at least one device is positioned outside of the room, omitting indoor configurations. Therefore, while existing studies shed light on deployment issues, there remains a need to comprehensively address the dynamic effects of walls and consider diverse deployment scenarios to fully understand and optimize sensing coverage in indoor environments.

This paper focuses on examining the impact of walls on sensing coverage in scenarios where all devices are located inside a room. Both theoretical analysis and experimental investigations are conducted to understand how walls influence the sensing capabilities. The results reveal that the performance of Wi-Fi sensing is significantly affected by the distance between the wall and the sensors. Fig. 1 illustrates that by reducing the distance between the wall and the Tx, the sensing coverage area can be expanded. Interestingly, the effect of walls on sensing is more intricate than previously assumed. Whether a wall enhances or reduces the sensing capability depends on the placement of the sensing devices relative to the wall. Consequently, walls can be strategically utilized to address the challenges of limited sensing coverage and enhance the robustness of the sensing system—the two most critical issues associated with wireless sensing. This study represents an important advancement towards the practical implementation of wireless sensing in real-world scenarios.

The main contributions of this work are as follows:

- This paper investigates the impact of wall reflection on Wi-Fi systems in indoor environments, which, to the best of our knowledge, has not been explored before. Our findings reveal a positive effect of walls on sensing, highlighting their potential for enhancing wireless sensing capabilities. Given the prevalence of walls in indoor environments, our proposed model represents a significant step towards considering suitable device deployment strategies to enhance wireless sensing performance in real-world indoor scenarios.
- We present a novel wall-reflection sensing coverage model that incorporates two dynamic paths within indoor environments. Unlike previous sensing coverage models that only account for the direct path from devices to targets, the inclusion of reflected paths in our model results in an expanded sensing region. This expansion

occurs as the distance between the wall and the device decreases within a specific range, aligning more closely with real-world scenarios compared to previous models.

- This paper presents experimental results showcasing the practical effectiveness of our proposed model in expanding sensing coverage for stationary crowd counting applications. By strategically positioning the devices with respect to the walls, we demonstrate a notable improvement of 11.2% in the accuracy of stationary crowd counting. These empirical findings highlight the tangible benefits of applying our model, providing valuable insights for optimizing device placement and enhancing the performance of wireless sensing systems in real-world scenarios.

The rest of this paper is organized as follows. In Section 2, we provide a brief overview of the related work in the field. Section 3 presents the preliminary knowledge related to the proposed model. The model itself, along with its properties, is detailed in Section 4 and Section 5. In Section 6, we present the experimental results that validate the accuracy and usefulness of the proposed model. We discuss the limitations of our approach and potential directions for future work in Section 7 and conclude our work in Section 8.

II. RELATED WORK

This section provides a concise overview of existing research on the sensing coverage of RF-based contactless sensing systems, summarizing the key findings and developments in this field.

A. Modeling sensing coverage in free space

Extensive research has been conducted on the sensing coverage of radar systems, primarily focusing on free space conditions. Yang et al. [19] explored the geometrical relationship between the coverage area of a bistatic radar and the distance between the transmitter and receiver. Similar investigations have been carried out in Wi-Fi systems, where Xin et al. [20] developed a sensing coverage model for different movement patterns in free space, utilizing a Fresnel zone model. The size of the sensing coverage was found to be influenced by the extent of the target's reflection surface, with larger reflection surfaces resulting in expanded sensing coverage.

Wang et al. [17] proposed a sensing coverage model based on sensing capability metrics, observing that coverage size initially increases but eventually decreases with increasing distances between the transmitter and receiver.

While existing studies have delved into sensing coverage in indoor scenarios, none of them considers the reflection effect of walls on targets. Walls are commonly viewed as obstacles in indoor environments, affecting only the static power in the sensing coverage model. This paper, however, accounts for the effects of walls on the dynamic power and explores the phase interactions between the wall-reflected path and the LoS path within the sensing coverage model.

B. Modeling sensing coverage with blocks

There have been research endeavors that consider non-line-of-sight (NLoS) scenarios, such as through-wall sensing, when developing sensing coverage models. Zhang et al. [21] proposed a through-wall wireless sensing model utilizing the Fresnel zone concept to characterize the sensing mechanisms of Wi-Fi signals in through-wall scenarios. Their refraction-aware Fresnel model demonstrated that the presence of walls can enhance through-wall sensing capabilities. Woodford et al. [22] employed curved reflectors and planar surfaces to achieve comprehensive coverage and enable NLoS radar sensing in crucial areas near intersections. Xie et al. [18] developed a through-wall sensing model with LoRa systems, leveraging walls to expand sensing coverage and mitigate interference.

The aforementioned studies focus on the impact of walls on through-wall sensing scenarios, where their models necessitate that at least one of the devices or targets be located on the other side of the wall, considering only a single signal path through the wall. In contrast to these works, our research delves into wall-reflected signals with both devices and targets positioned within the indoor environment, rather than the through-wall scenario. Our objective is to investigate how the integration of wall-reflected signals and LoS signals influences the dynamic power, and hence the sensing coverage region.

III. PRELIMINARIES

In this section, we introduce the basics of CSI-based sensing, and the sensing coverage model without walls.

A. Channel State Information

In an indoor environment, Wi-Fi signals can encounter numerous obstacles such as walls and human bodies, resulting in signal reflections and multiple paths to reach the receiver. These paths can be categorized into two types: static paths and dynamic paths, as depicted in Fig. 2. Static paths encompass the line-of-sight (LoS) path and paths reflected from stationary objects, while dynamic paths are generated by changes in target objects, such as human movements. CSI is utilized to characterize the wireless channel between a transmitter and a receiver in Wi-Fi systems [23]. The received signal can be mathematically represented by

$$Y(f, t) = H(f, t) \times X(f, t), \quad (1)$$

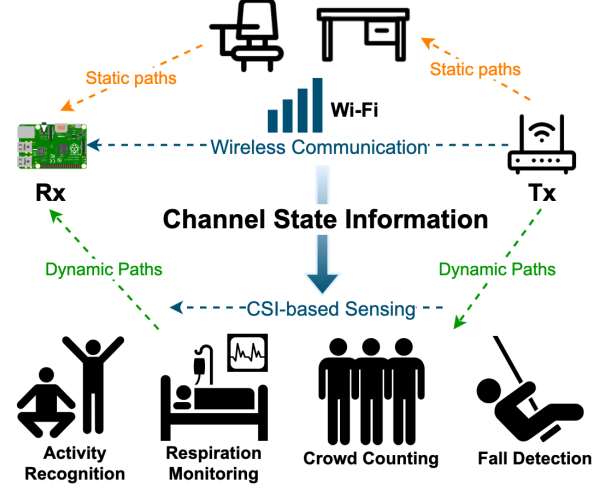


Fig. 2. Categorizing Wi-Fi signal propagation: static paths vs dynamic paths.

where $X(f, t)$ and $H(f, t)$ denote respectively the frequency domain representations of the transmitted signal and the complex-valued channel frequency response (CFR) at carrier frequency f and time t . Within the CSI matrix, each individual element can be represented as a linear combination of all the signal paths, which can be demonstrated as

$$\begin{aligned} H(f, t) &= H_s(f, t) + H_d(f, t) + H_n(f, t) \\ &= |H_s(f, t)| e^{-j\theta_s} + |H_d(f, t)| e^{-j\theta_d} \\ &\quad + |H_n(f, t)| e^{-j\theta_n}, \end{aligned} \quad (2)$$

where H_s denotes the contribution of the static path, H_d represents the dynamic path, and H_n corresponds to the noise component. The amplitude of each CSI component is denoted by $|H|$, while θ indicates the phase [24]. By decomposing the CSI matrix in this manner, we can effectively analyze and understand the contributions of different signal paths to the overall wireless channel characteristics.

B. Sensing Coverage Model without Walls

A metric named SSNR (sensing-signal-to-noise-ratio) was proposed by Wang et al. [17] to quantify the sensing capability:

$$SSNR = \frac{P_d}{P_i} = \frac{P_d}{\gamma P_{LoS} + b}, \quad (3)$$

where P_d is the power of the dynamic signal, P_i is the interference power, which is linearly proportional to the static power P_{LoS} . It is worth noting that the static path is assumed to be the LoS path, and the power of the LoS signal can be mathematically expressed using the Friis equation [25]–[27] as

$$P_{LoS} = \frac{P_T G_T A_R}{4\pi(r_D)^2}, \quad (4)$$

where P_T represents the transmission power, G_T indicates the antenna gain of the transmitter, and r_D represents the

distance between the transmitter and receiver. A_R corresponds to the effective aperture of the receiver's antenna, which can be calculated as $A_R = \frac{G_R \lambda^2}{4\pi}$, with G_R denoting the antenna gain of the receiver and λ representing the wavelength of the signal. However, in real indoor scenarios, the static path includes reflections from other stationary objects, which can lead to variations in the interference power P_i [17].

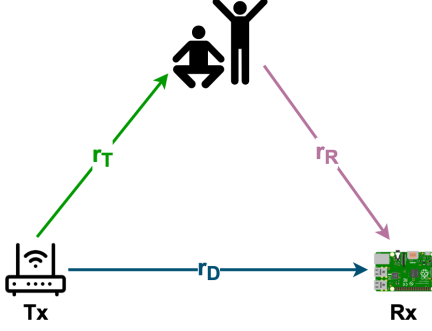


Fig. 3. Sensing model without walls.

Consider a simple scenario in free space, the dynamic path can be divided into two parts as shown in Fig. 3. The first part with a distance r_T is the signal from the transmitter to the target, and the second part with a distance r_R is the reflected signal from the target to the receivers. According to the Friis equation [25], the power of the signal arriving at the target can be expressed as

$$P_{r_T} = \frac{P_T G_T}{4\pi(r_T)^2}. \quad (5)$$

The power of the signal reflected by the target and received by the receiver can be mathematically expressed as

$$P_{r_R} = \frac{P_{r_T} \sigma A_R}{4\pi(r_R)^2} = \frac{P_T G_T \sigma A_R}{(4\pi)^2 (r_T r_R)^2}, \quad (6)$$

where σ represents the radar cross section (RCS) of the target, encompassing the effective reflection ratio at the target [28]. In free space, the power of the dynamic signal P_d equals to P_{r_R} . Therefore, the $SSNR_{LoS}$ can be expressed as

$$SSNR_{LoS} = \frac{P_{r_R}}{\gamma P_{LoS} + b} = \frac{K \sigma}{(4\pi)(r_T r_R)^2 (\gamma \frac{K}{r_D^2} + b)}, \quad (7)$$

where $K = \frac{P_T G_T A_R}{4\pi}$. According to the findings in [17], the variables γ and b have fixed values for a given pair of Wi-Fi transceivers. Furthermore, the transmission power P_T , antenna gains G_T and G_R , and signal wavelength λ are assumed to be constant. Assuming a constant RCS of the target σ and a small value for b , (7) can be simplified as

$$SSNR_{LoS} \propto \frac{r_D^2}{(r_T r_R)^2}. \quad (8)$$

The derived equation demonstrates the close relationship between the sensing capability and various distances, namely the distances of the target reflection signal (r_T and r_R) and

the distance between the transceivers (r_D). By considering the minimum SSNR requirement, we can express the boundary of the sensing area as

$$(r_T r_R)_b \propto \sqrt{\frac{r_D^2}{SSNR_{min}}}. \quad (9)$$

Note that the minimum SSNR requirement $SSNR_{min}$ varies with sensing applications and signal preprocessing methods. From (9), we can see that the sensing area initially increases and then decreases as the length of the LoS path increases.

IV. UNDERSTANDING THE EFFECT OF WALLS ON INDOOR SENSING SYSTEMS

The sensing coverage model outlined in [17] primarily concentrates on free space scenarios, acknowledging walls as obstacles that solely impact static power. Nevertheless, when devices or targets are close to walls, the influence of signals reflected by walls on dynamic power becomes significant. In response, we have developed a novel model customized for multipath-dominant indoor environments. This model accounts for the impact of walls and factors in the distances between the Tx and Rx, to precisely evaluate indoor sensing capabilities.

Fig. 4 illustrates three common wall-reflection scenarios encountered in indoor environments: i) when the transmitter is deployed in close proximity to the wall (Fig. 4a); ii) when the receiver is deployed in close proximity to the wall (Fig. 4b); and iii) when both the transmitter and receiver are deployed in close proximity to the wall (Fig. 4c). In this paper, we focus on the scenario depicted in Fig. 4a to demonstrate the impact of wall reflection. However, the theories and findings presented in this paper are applicable to the scenarios in Fig. 4b and Fig. 4c as well.

A. Wall-reflection Sensing Model

When there is a wall close to the transmitter, parts of the signals will be reflected by the wall before arriving at the target as shown in Fig. 4a. We can divide the wall-reflected signal into two parts: from the Tx to the wall with a distance d_1 and reflected by the wall to the target with a distance d_2 . Based on the Friis equation [25]–[27], the power of the signal arriving at the wall can be expressed as

$$P_{d_1} = \frac{P_T G_T}{4\pi(d_1)^2}, \quad (10)$$

where P_T represents the transmission power and G_T denotes the antenna gain of the transmitter. The power of the signal reflected by wall to the target can be mathematically expressed as

$$P_{d_2} = \frac{P_{d_1} R_{wall}^2}{4\pi(d_2)^2} = \frac{P_T G_T R_{wall}^2}{(4\pi)^2 (d_1 d_2)^2}, \quad (11)$$

where R_{wall} is the reflection coefficient of the wall [29], [30]. The power of the signal reflected by the target and arriving at the receiver can be expressed as

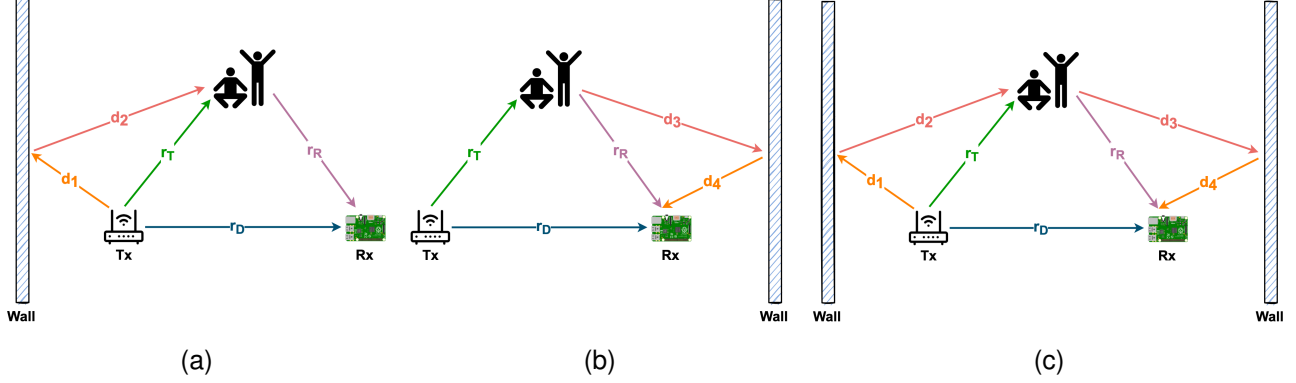


Fig. 4. Wall-reflection sensing model. (a) Tx near the wall. (b) Rx near the wall. (c) Both Tx and Rx near walls.

$$P_{rR} = \frac{P_{d2} \sigma A_R}{4\pi (r_R)^2} = \frac{P_T G_T R_{wall}^2 \sigma A_R}{(4\pi)^3 (d_1 d_2 r_R)^2}, \quad (12)$$

where σ represents the RCS of the target, encompassing the effective reflection ratio at the target [28]. A_R corresponds to the effective aperture of the receiver's antenna, which can be calculated as $A_R = \frac{G_R \lambda^2}{4\pi}$, with G_R denoting the antenna gain of the receiver and λ representing the wavelength of the signal.

Assume that the static path is the LoS path, and the power of the LoS signal is the same as (4):

$$P_s = \frac{P_T G_T A_R}{4\pi (r_D)^2}, \quad (13)$$

where r_D represents the distance between the transmitter and receiver. To incorporate the impact of wall reflections on indoor environments, the $SSNR_{LoS}$ proposed in [17] can be adapted using the following formula:

$$SSNR_{wall} = \frac{P_{rR}}{\gamma P_s + b} = \frac{K R_{wall}^2 \sigma}{(4\pi)^2 (d_1 d_2 r_R)^2 (\gamma \frac{K}{r_D^2} + b)}, \quad (14)$$

where $K = \frac{P_T G_T A_R}{4\pi}$. By considering that K and γ are constants, and assuming a constant RCS of the target σ , a constant reflection coefficient of the wall R_{wall} , and a small value for b , (14) can be simplified as

$$SSNR_{wall} \propto \frac{r_D^2}{(d_1 d_2 r_R)^2}. \quad (15)$$

From this equation, we can see that the sensing capability is closely related to the distances of the target-reflected signal (d_1 , d_2 , and r_R) and the distance of the static signal (r_D). It also provides a means to investigate how the sensing capability changes with varying target locations. Notably, regions close to the devices and the wall demonstrate higher sensing capabilities. This implies that targets situated in close proximity to these regions are more likely to be accurately detected.

However, it is important to note that this model solely considers the dynamic signals resulting from the reflection off the wall. In Section IV-B, we will further explore the impact of the dominant target reflected signals originating from the LoS signals.

B. The Sensing Coverage Model in Indoor Environments Considering the Effect of Walls

While the presence of walls does affect the dynamic power in indoor environments, it is important to note that the paths with r_T and r_R depicted in Fig. 4 continue to play a dominant role in the dynamic paths. To create a comprehensive model for indoor environments, we can incorporate the wall-reflected paths d_1 and d_2 along with the existing paths to calculate the overall dynamic power accurately. By considering these combined paths, we can develop a comprehensive model that accounts for both LoS and wall-reflected signals in indoor environments.

According to [31], the combined dynamic power can be expressed as

$$\begin{aligned} P_d &= P_{d_{wall}} + P_{d_{LoS}} + 2\sqrt{P_{d_{wall}} P_{d_{LoS}}} \cos(\Delta\phi) \\ &= \frac{P_T G_T R_{wall}^2 \sigma A_R}{(4\pi)^3 (d_1 d_2 r_R)^2} + \frac{P_T G_T \sigma A_R}{(4\pi)^2 (r_T r_R)^2} \\ &\quad + \frac{2P_T G_T R_{wall} \sigma A_R \cos(\Delta\phi)}{(4\pi)^{\frac{5}{2}} (r_R)^2 (d_1 d_2 r_T)}, \end{aligned} \quad (16)$$

where $P_{d_{wall}}$ is expressed in (12) and $P_{d_{LoS}}$ is expressed in (6). The phase difference between the two signals can be expressed as $\Delta\phi = \frac{2\pi(d_1 + d_2 - r_T)}{\lambda}$, where λ is the signal wavelength. As the static power P_s is shown in (13), the SSNR can be expressed as

$$\begin{aligned} SSNR &= \frac{P_d}{P_i} = \frac{P_{d_{wall}} + P_{d_{LoS}} + 2\sqrt{P_{d_{wall}} P_{d_{LoS}}} \cos(\Delta\phi)}{\gamma P_s + b} \\ &= \frac{K R_{wall}^2 \sigma}{(4\pi)^2 (d_1 d_2 r_R)^2 (\gamma \frac{K}{r_D^2} + b)} \\ &\quad + \frac{K \sigma}{4\pi (r_T r_R)^2 (\gamma \frac{K}{r_D^2} + b)} \\ &\quad + \frac{2K R_{wall} \sigma \cos(\Delta\phi)}{(4\pi)^{\frac{3}{2}} (r_R)^2 (d_1 d_2 r_T) (\gamma \frac{K}{r_D^2} + b)}, \end{aligned} \quad (17)$$

where $K = \frac{P_T G_T A_R}{4\pi}$. By considering that K and γ are constants, and assuming a constant RCS of the target σ , and a small value for b , (17) can be simplified as

$$\begin{aligned}
SSNR &\propto \frac{\alpha_1(r_D)^2}{(d_1d_2r_R)^2} + \frac{(r_D)^2}{(r_Tr_R)^2} + \frac{\alpha_2\cos(\Delta\phi)(r_D)^2}{(d_1d_2r_T)(r_R)^2} \\
&= \alpha_1 SSNR_{wall} + SSNR_{LoS} \\
&\quad + \alpha_2 \frac{\cos(\Delta\phi)(r_D)^2}{(d_1d_2r_T)(r_R)^2},
\end{aligned} \tag{18}$$

where $SSNR_{wall}$ is shown in (15) and $SSNR_{LoS}$ is shown in (8). Parameters $\alpha_1 = \frac{R_{wall}^2}{4\pi}$ and $\alpha_2 = \frac{R_{wall}}{\sqrt{\pi}}$, where the reflection coefficient R_{wall} varies with different wall materials and incident angles [30].

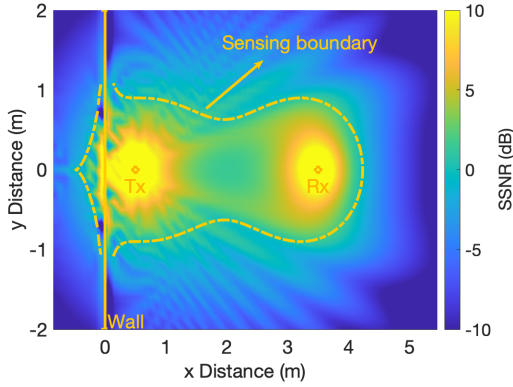


Fig. 5. Heatmap of sensing capability in indoor environments.

Fig. 5 illustrates the heatmap of the sensing capability based on our proposed model in (18) with a Wall-Tx distance of 0.5 m. Based on our analysis, variations in the reflection coefficient do not have significant impact on the characteristics of this model; therefore, we adopt a reflection coefficient of 0.3 [32]. This model integrates the dynamic signals from LoS conditions and reflections off the wall. The heatmap employs a color scheme where yellow indicates higher sensing capability, while blue represents lower sensing capability. The rapid fluctuations between the light and dark colors are caused by the phase interactions between the two paths. However, this phenomenon is negligible compared to the dominant sensing regions near the wall and devices. Upon observing the heatmap, we notice that areas in proximity to the devices and the wall exhibit higher sensing capability. This suggests that targets located near these areas are more likely to be effectively detected.

For the sensing boundary, we consider a minimum SSNR requirement of 2 dB for reliable sensing, as established in previous works [17], [18]. Due to the phase interplay between the two signal paths, the actual sensing boundaries manifest as zigzag patterns. To facilitate easier computation of the sensing area, the visualized sensing boundary is smoothened, as demonstrated in Fig. 5. By examining (18), we can observe that both the Tx-Rx distance and the wall-device distance play significant roles in determining the sensing boundary. The area of the region with the same SSNR expands as the device gets closer to the wall. In Section V, we will delve deeper into the analysis of this sensing boundary, considering the aforementioned distances to provide additional insights.

V. ENHANCING SENSING COVERAGE IN INDOOR ENVIRONMENTS WITH WALLS

In this section, we investigate the fundamental factors that impact the sensing coverage in the presence of wall reflections. We aim to understand how these factors can be effectively managed to address two prominent issues in wireless sensing: limited sensing coverage and instability due to interference. By analyzing and controlling the sensing coverage, we can mitigate the challenges posed by these issues and enhance the overall performance of wireless sensing systems.

A. Factors affecting sensing coverage

According to the sensing coverage model discussed in Section IV-B, the shape and size of the sensing coverage are significantly influenced by two primary factors: the distance between the wall and the devices and the distance between the transmitter and receiver.

Factor I: Wall-Device Distance.

We initially investigate the effect of the wall-device distance on the sensing boundary. Fig. 6 depicts the smoothened sensing boundary of a Wi-Fi sensing system with various distances between the wall and the transmitter, based on our analytical model in (18). It should be noted that we use an SSNR threshold of 2 dB to represent the sensing boundary, but the actual minimum SSNR required for sensing at the boundary may vary depending on the specific application, signal preprocessing techniques, and static power considerations. We maintain a fixed distance of 3 m between the Tx and Rx and increase the wall-transmitter distance from 0.1 m to 2.5 m. To ensure that only the wall-transmitter distance is altered, we simultaneously move both the Tx and Rx. As shown in Fig. 6a, Fig. 6b, and Fig. 6c, when the device is closer to the wall, the shape of the sensing coverage is affected by the wall and no longer like a Cassini oval [17] with (8). As the distance between the wall and the devices becomes larger, the impact of the wall on the sensing coverage diminishes. When the distance exceeds a certain threshold, such as 2 m shown in Fig. 6e, the shape and size of the sensing coverage closely resembles the sensing coverage model without a wall.

Based on this observation, we can conclude that the sensing coverage becomes larger when the devices are positioned closer to the wall within a certain range. However, when the device is too close to the wall, as depicted in Fig. 6a, the sensing coverage on the other side of the wall also increases. The expansion of the sensing coverage beyond the wall can lead to increased interference and adversely affect the performance, especially when there are other objects present on the other side of the wall. The underlying reason for this phenomenon is explained in the through-wall model proposed in [18]. We will further evaluate and analyze this property in Section VI-B.

Factor II: Transmitter-Receiver Distance.

To examine the impact of the Tx-Rx distance, we maintain the distance between the wall and transmitter at 1 m and move the receiver to increase the Tx-Rx distance from 0.1 m to 5 m. As illustrated in Fig. 7, the corresponding sensing coverage initially increases and then decreases and separates into two

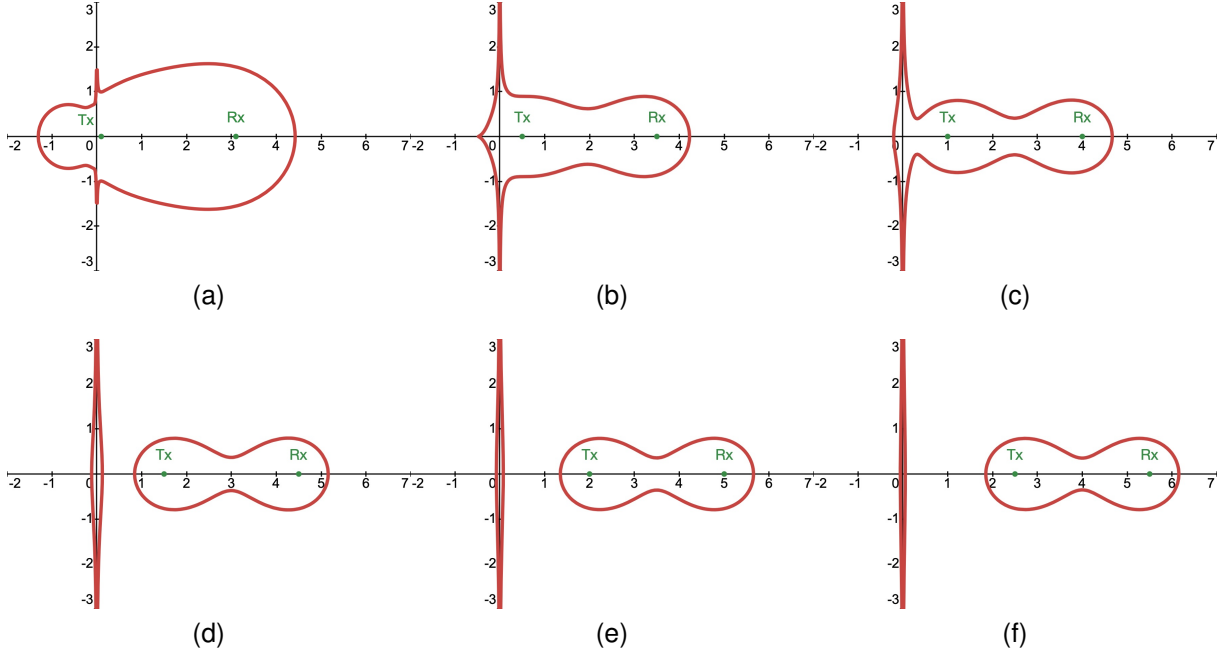


Fig. 6. The sensing coverage boundary under different Wall-Tx distances. (a) Wall-Tx distance: 0.1 m. (b) Wall-Tx distance: 0.5 m. (c) Wall-Tx distance: 1 m. (d) Wall-Tx distance: 1.5 m. (e) Wall-Tx distance: 2 m. (f) Wall-Tx distance: 2.5 m.

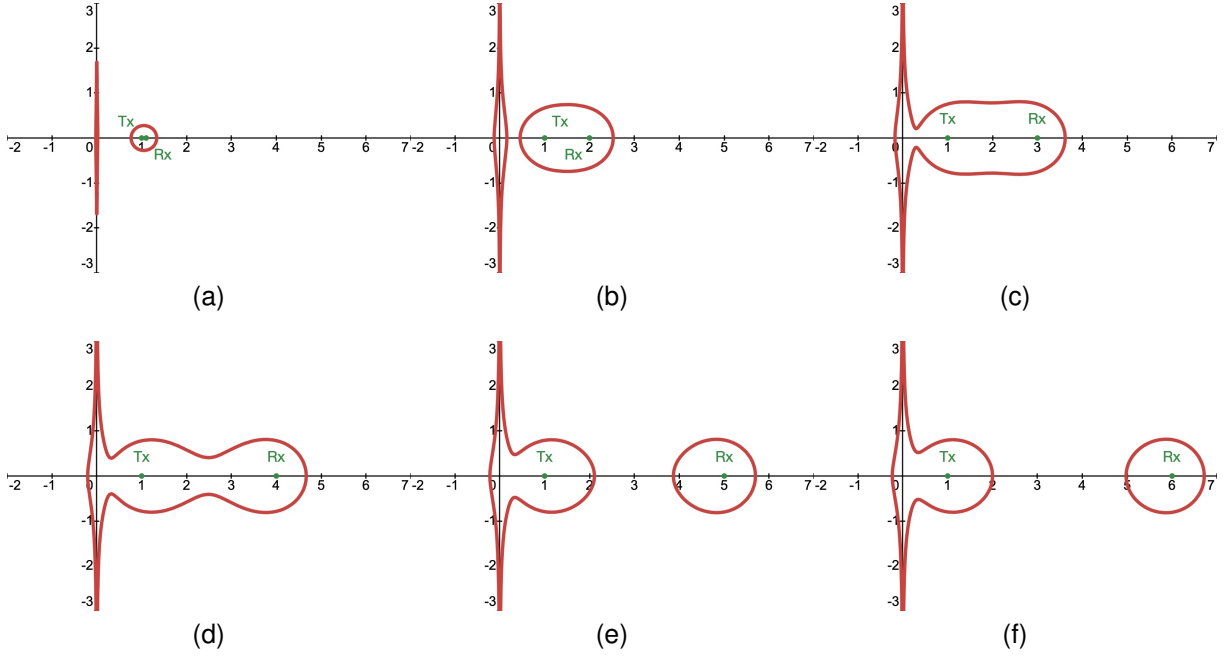


Fig. 7. The sensing coverage boundary under different Tx-Rx distances. (a) Tx-Rx distance: 0.1 m. (b) Tx-Rx distance: 1 m. (c) Tx-Rx distance: 2 m. (d) Tx-Rx distance: 3 m. (e) Tx-Rx distance: 4 m. (f) Tx-Rx distance: 5 m.

distinct parts as the Tx-Rx distance increases. Specifically, when the distance is less than 3 m, the sensing coverage has an oval shape, and the coverage area expands as the Tx-Rx distance increases. However, when the distance exceeds 4 m, as depicted in Fig. 7e, the sensing coverage transforms into two circular regions surrounding the transceivers. Notably, the device situated closer to the wall exhibits a slightly larger sensing coverage compared to the device farther away from

the wall. This discrepancy primarily arises from the increased dynamic power resulting from wall-reflected signals.

B. Key Properties of the Indoor Sensing Coverage Model

Based on the above theoretical analysis, we can summarize the key properties of Wi-Fi sensing coverage in indoor environments with respect to the wall-reflection effect as follows:

- 1) Whether walls have effects on the sensing coverage in Wi-Fi systems is dependent on the locations of devices relative to walls. When the distance between the device and the wall exceeds a threshold (e.g., 2 m in Fig. 6), the sensing capability takes the shape of Cassini ovals.
- 2) When the distance between the wall and the device is short (e.g., 0.1 to 1 m in Fig. 6), as the distance decreases, the sensing coverage expands both within the room and outside the room (on the other side of the wall).
- 3) When the distance between the wall and the device is moderate (e.g., 1 - 2 m in Fig. 6), the wall still has some effect on the sensing coverage inside the room, while the effect on the sensing coverage outside the room, beyond the walls, becomes negligible.
- 4) When the transmitter-receiver distance is small (e.g., 0.1 - 3 m in Fig. 7), the size and shape of the sensing coverage is a single small area. When the transmitter-receiver distance is large (e.g., > 4 m in Fig. 7), the size and shape of the sensing coverage becomes several separated small areas surrounding the wall, transmitter, and receiver.

VI. EVALUATION

In this section, our focus is on validating the key properties of the indoor sensing coverage model through two specific applications. First, respiratory monitoring is employed to evaluate the effectiveness of the SSNR-based model regarding its sensing capabilities. Second, stationary crowd counting is utilized to assess the sensing coverage properties of the proposed model. The experiments conducted on these applications provide a foundation for our subsequent analysis, allowing us to validate the reliability and accuracy of our findings. Leveraging the properties obtained from these experiments, we then utilize them to guide the system design of stationary crowd counting with various scenarios.

Hardware Setup. In the conducted experiments, a router with omni-directional antennas was used as the transmitter, while a Raspberry Pi equipped with the Nexmon CSI Extraction Tool [33] served as the receiver. The employed tool is able to support 802.11a/g/n/ac transmissions in both the 2.4 and 5 GHz bands, with a maximum bandwidth of 80 MHz. To maximize the available information, we utilized the 80 MHz bandwidth in the 5 GHz band, capturing 242 subcarriers after removing nulls. Since the Raspberry Pi has a single antenna and its Wi-Fi chip operates on a single core, each Pi collected a single CSI matrix. The sampling frequency was set to 1000 Hz. In order to ensure stability, the transceivers were mounted on tripods at a height of 1 m. Fig. 8 provides an example of the experimental setup in a meeting room.

Evaluation Setup. The key of this paper is to demonstrate the improvement contributed by the effect of walls, and the relationship between the proposed model and the performance of sensing applications in real scenarios. In the context of respiratory monitoring, our methodology integrates signal processing techniques such as the Hampel filter [34], Savitzky-Golay filter [35], and peak detection algorithms to compute respiratory

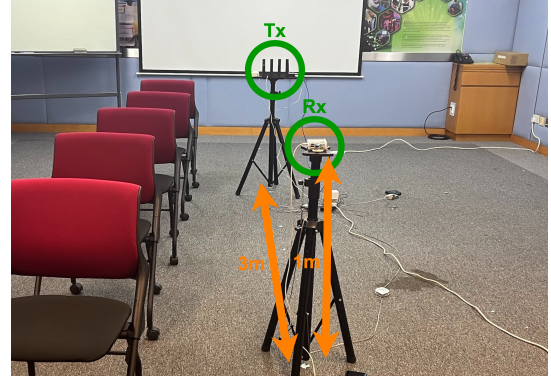


Fig. 8. Hardware setup in a real scenario.

rates in breaths per minute (bpm). A reference respiration rate is acquired from a Neulog Respiration Monitor Belt logger sensor NUL236. The Mean Absolute Error (MAE) metric [36] is employed to evaluate the application performance.

For stationary crowd counting accuracy evaluations, we leverage traditional machine learning models, namely Support Vector Machines (SVM), Random Forest (RF), and K-Nearest Neighbors (KNN). The preprocessing methods and parameters employed in these models remained consistent with our previous research [37]. Although more advanced signal processing and deep learning methods have the potential to achieve accuracy rates exceeding 99%, our objective is to analyze the unique enhancements provided by our sensing coverage model, which necessitates a comparative analysis against established benchmarks. Thus, we chose to utilize simple approaches to facilitate a meaningful and efficient assessment of the enhancements achieved.

A. Evaluating Sensing Capability of the Proposed Model through Respiratory Monitoring

To validate the properties of the proposed model concerning sensing capability, we conducted experiments specifically tailored for respiration monitoring applications. We compared the simulated SSNR, the real-scenario SSNR, and the MAE results in various scenarios.

For the real-scenario SSNR, the dynamic power is computed based on the disparity between the CSI amplitude and the averaged amplitude within the observation window. The interference power is determined as the difference before and after filtering the CSI amplitude [17]. In Fig. 9, a respiration example is illustrated with different Wall-Tx distances. When the device is near the wall (Fig. 9a), the variance in the CSI amplitude increases, while the noise before and after filtering decreases, indicating a higher SSNR value.

Experiment 1: Verify the effectiveness of using simulated SSNR to assess SSNR measured in real scenarios

In this experiment, the data with a single target respiring at various locations is examined. Fig. 10 illustrates the comparison between the simulated SSNR and the SSNR derived from real-world data. It is evident that the SSNR in the real scenario aligns with the simulated SSNR by a scale factor. This factor is contingent upon parameters such as device

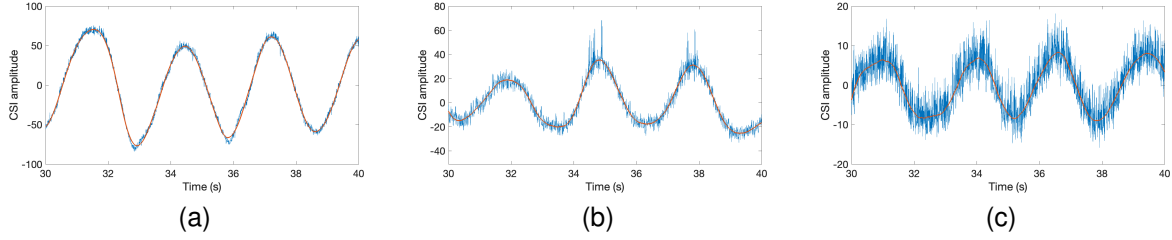


Fig. 9. The respiratory signal under different Wall-Tx distances. (a) Wall-Tx distance: 0.1 m. (b) Wall-Tx distance: 0.5 m. (c) Wall-Tx distance: 1 m.

power, transceiver deployment, and environmental conditions. In our simulated model, we normalized the effect of these parameters, as they do not significantly impact the correlation between wall, device, target distances, and sensing coverage. These results validate the efficacy of our proposed SSNR-based model in assessing sensing capability and coverage.

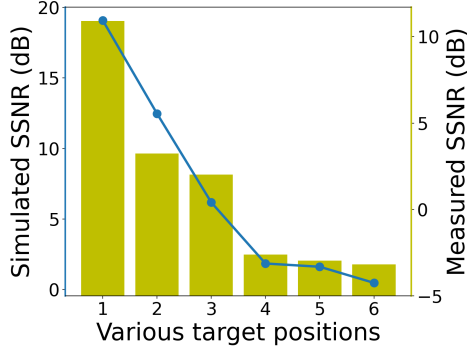


Fig. 10. Verify the effect of the SSNR metric with a target in various positions.

Experiment 2: Verify the effect of the wall-device distance without interference

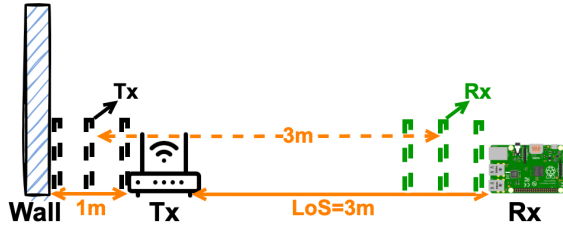


Fig. 11. Verify the effect of the wall-device distance by moving transceivers at the same time.

In this experiment, we aim to verify the impact of the wall-device distance on the sensing capability. We position the transmitter at distances of 0.1 m, 0.5 m, and 1 m away from the wall, as depicted in Fig. 11. The distance between the Tx and Rx is fixed at 3 m, with the Rx moving simultaneously with the Tx. Fig. 12 presents the MAE (line chart) obtained for the three cases, along with the corresponding SSNR value (bar chart). We observe that the experimental result aligns well with the simulation trend. Specifically, as the distance between the wall and the device decreases within a limited range, the sensing capability increases, and the MAE decreases. This finding

confirms the relationship between the wall-device distance and the extent of the sensing capability, as predicted by the simulation analysis.

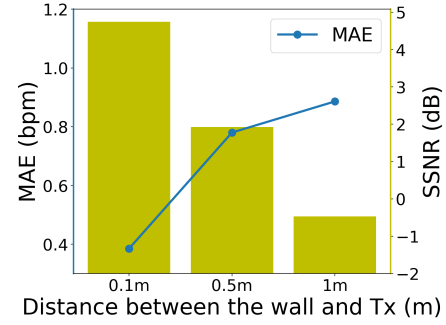


Fig. 12. Evaluation results of the effect of the wall-device distance without interference.

Experiment 3: Verify the effect of the wall-device distance with interference

The aim of this experiment is to verify the impact of the wall-device distance on sensing area expansion and its potential negative effect when interferers are present within this expanded area. The experimental setup mirrors that of Experiment 2, with the addition of an interferer within the sensing area. In Fig. 13, the green bars depict SSNR values in real scenarios, while the blue line represents the MAE for the target within the room.

As the transmitter moves closer to the wall, the SSNR decreases, indicating significant interference in this case. The trend observed in Fig. 13 demonstrates that as the wall-device distance increases, the MAE decreases. This pattern validates the adverse impact of a short wall-device distance when interferers are present within the sensing range.

B. Evaluating Sensing Coverage of the Proposed Model through Stationary Crowd Counting

To validate the sensing coverage aspects of the proposed model, we conducted experiments tailored specifically for stationary crowd counting applications. By dispersing multiple targets randomly throughout the entire space during the experiment, we can effectively discern properties associated with sensing coverage. In this scenario, we validate the model and the simulated sensing boundary by correlating them with the counting accuracy. Higher accuracy indicates better performance, implying a larger sensing coverage area in the

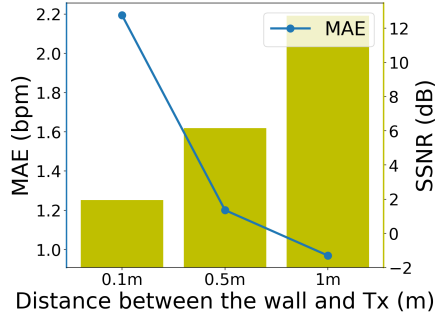


Fig. 13. Evaluation results of the effect of the wall-device distance with interference.

deployment. While the real sensing area expands beyond the simulated area due to advanced signal preprocessing methods, the trends observed with varying device positions should still align with the simulated model.

Experiment 1: Verify the effect of the wall-device distance without interference

In this experiment, we aim to verify the impact of the wall-device distance on the sensing coverage, as discussed in Section V-A. The device deployment settings are the same as in Section VI-A, as depicted in Fig. 11. Fig. 14 presents the accuracy results (line charts) obtained for the three cases, along with the corresponding simulation-based sensing areas (bar chart). We observe that the experimental results across all three models align well with the simulation trend. Specifically, as the distance between the wall and the device decreases within a limited range, the indoor sensing area increases. This finding confirms the relationship between the wall-device distance and the extent of the sensing coverage, as predicted by the simulation analysis.

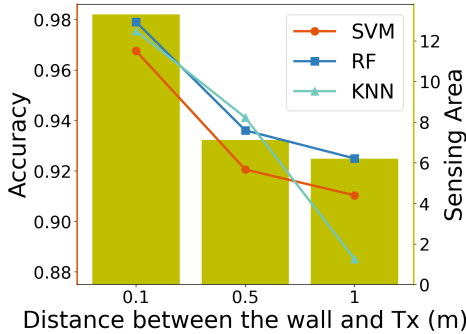


Fig. 14. Evaluation results of the effect of the wall-device distance without interference.

Experiment 2: Verify the effect of the wall-device distance with interference

As mentioned in Section IV-B, when the device is close to the wall, the sensing area on the other side of the wall also increases, which will have a negative effect on indoor sensing applications. This experiment is designed to verify this property. The experiment setup is the same as Experiment 1 except that there are people outside the room and close to the wall. In Fig. 15, the green bars represent the sensing areas beyond the wall and the three lines show the accuracy

results across all three models for people counting within the room. As the Tx moves closer to the wall, the sensing area on the other side of the wall extends, which indicates a large interference area in this experiment. As can be seen from Fig. 15, with an increase in the wall-device distance, the accuracy increases. This trend verifies the negative effect of a short wall-device distance when there are interferers beyond the wall.

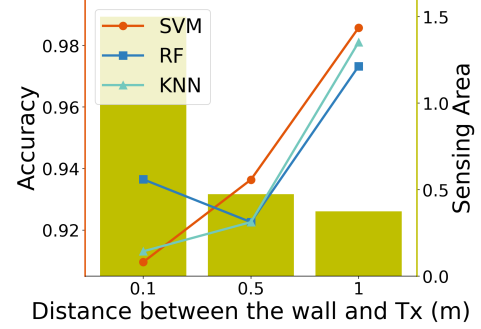


Fig. 15. Evaluation results of the effect of the wall-device distance with interference.

Experiment 3: Verify the effect of the transmitter-receiver distance

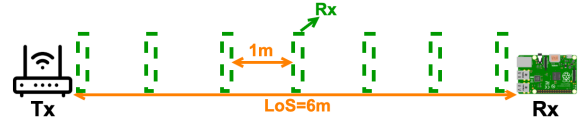


Fig. 16. Verify the effect of the Tx-Rx distance by placing the transceivers at different locations.

To evaluate the effect of the transmitter-receiver distance on the proposed model, we conducted experiments in a meeting room with a fixed distance of 1.2 m between the wall and the Tx. As depicted in Fig. 16, we varied the distance between the transceivers from 0 m to 6 m at a step size of 1 m. The results, shown in Fig. 17, indicate that the accuracy initially increases and then slightly decreases with the increased distance between the Tx and Rx. This trend is consistent across all the three models, and it aligns with the simulated sensing area presented in the bar chart. Notably, an optimal distance of 3 m emerged, resulting in the largest sensing area and the highest accuracy for stationary crowd counting in this particular environment. These experimental results serve to validate the property of the proposed model detailed in Section V-A.

C. Boosting the Sensing Coverage of Stationary Crowd Counting

In this section, we conduct experiments with stationary crowd counting on various scenarios to evaluate the effectiveness of utilizing the properties outlined in this paper to expand the sensing coverage. We categorize the deployment strategies into two types: i) Ensuring that one of the transceivers remains in close proximity to the wall while maintaining an optimal

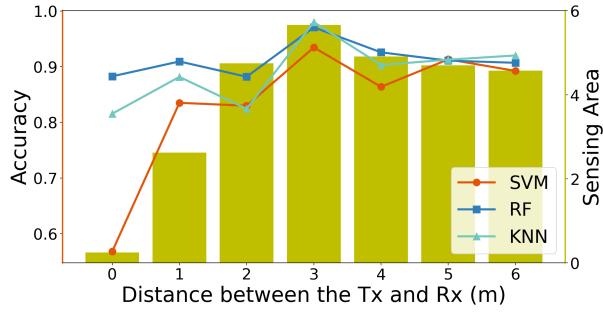


Fig. 17. Evaluation results of the effect of the Tx-Rx distance.

distance between the transceivers; and ii) Positioning both devices in close proximity to the walls.

Case 1: Scenarios where only one device is positioned close to the wall

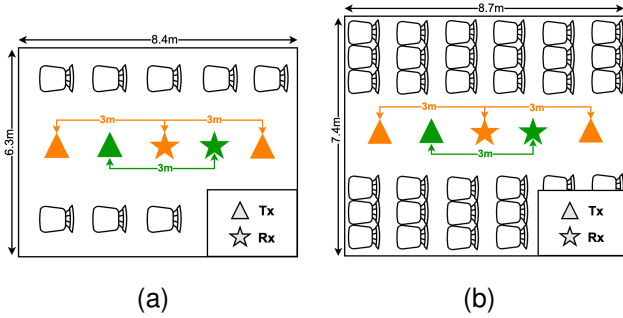


Fig. 18. Experiment setup in two indoor environments. (a) Meeting Room. (b) Classroom.

To expand the sensing coverage area inside the room and mitigate the negative effects of interference outside the room, based on the simulation model, we set the distance between the wall and the transmitter within the range of 1 m to 1.5 m. This deployment strategy is compared with a benchmark scenario where the transceivers are positioned at the center of the room. For each environment, in the benchmark setting, we maintain a larger distance of over 2.5 m between the wall and the transmitter. This comparison is motivated by the observation that, according to the proposed model, the influence of walls becomes negligible when the wall-device distance exceeds a certain threshold.

In this case, we conduct experiments in two distinct environments with different deployments, as depicted in Fig. 18. The green-colored topologies that are deployed at the center of the venues serve as benchmarks. The orange-colored topologies represent the four testing scenarios, which should generate larger sensing regions compared to the benchmarks. Due to variations in furniture arrangements in these two environments, the static power in these four scenarios differs.

Fig. 19 presents a comparison of the accuracy results for these scenarios. Each scenario includes a comparison between the benchmark configurations (center-aligned) and the topologies leveraging wall-reflected signals (side-aligned) using the three machine learning models (SVM, RF, KNN). The light-colored bars represent the benchmarks, while the dark-colored

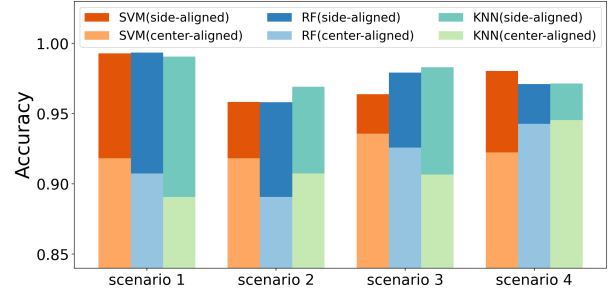


Fig. 19. Comparison of the counting accuracy under single-wall-proximity topologies and benchmarks in various scenarios.

bars indicate the improved accuracy attributed to the wall effect. Across all the scenarios, we observe that the accuracy of the case where the transmitter is positioned closer to the wall (light- and dark-colored) is consistently higher than the accuracy of the benchmark case (light-colored). This result also serves as further confirmation of the property that the wall has a positive effect on the sensing coverage when the distance between the wall and the device is within a certain range.

Case 2: Scenarios where both devices are positioned close to the wall

It is evident that the sensing area of the Wi-Fi system is quite limited if the placement of devices is not carefully planned. As shown in Fig. 20a, even when we deployed the optimal distance of 3 m between the transceivers in the meeting room, the sensing coverage did not encompass the entire room. To further enhance the sensing coverage, deploying both devices in close proximity to the walls can be a viable strategy, as illustrated in Fig. 20b. To evaluate the effect of this deployment strategy, we compare the sensing coverage by evaluating the accuracy of stationary crowd counting under three different scenarios:

- 1) In the first scenario, as shown in Fig. 20, the transceivers are horizontally placed in a meeting room. To expand the sensing coverage, we move the Tx and Rx in opposite directions within the room and deploy them near two sides of the room (walls).
- 2) In the second scenario, we maintain the same settings as in the first scenario but in a different environment—a classroom with a different size compared to the meeting room. As a result, the distance between the transceivers is distinct from the first scenario. This scenario is illustrated in Fig. 21.
- 3) In the third scenario, as depicted in Fig. 22, the transceivers are positioned vertically. In this case, we employ a different strategy to expand the sensing coverage. The Tx and Rx are moved synchronously, maintaining a fixed distance between them, and positioned close to the same side of the room (wall).

In each of the mentioned scenarios, we compare the deployment strategy with a benchmark where the transceivers are placed at the center of the room. This benchmark serves as a reference point for evaluating the effectiveness of boosting the sensing coverage through different deployment strategies.

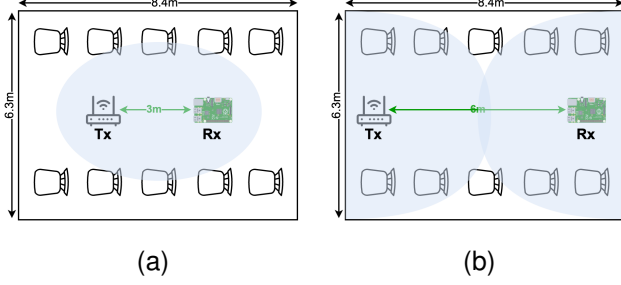


Fig. 20. Enlarging sensing coverage with devices in two sides (Meeting Room). (a) Benchmark. (b) Wall-proximity topology.

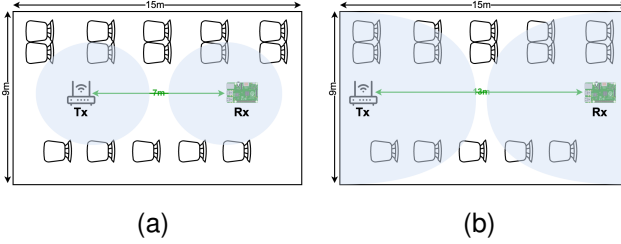


Fig. 21. Enlarging sensing coverage with devices in two sides (Classroom). (a) Benchmark. (b) Wall-proximity topology.

Based on the results shown in Fig. 23, it is evident that in all the three scenarios, the accuracy of crowd counting has been significantly improved by deploying the devices near the boundary of the room (dark-colored). This observation confirms the effectiveness of the deployment strategies in expanding the sensing coverage and enhancing the accuracy of stationary crowd counting. By leveraging the properties of the proposed model and strategically placing the transceivers close to the walls, we were able to achieve improved results in terms of detection accuracy in each of the scenarios.

VII. DISCUSSION

In this section, we acknowledge the limitations of our work and highlight potential future directions for further improvement and exploration.

Multiple walls. The proposed model currently considers the effect of only a single wall on dynamic power, whereas in reality, indoor spaces typically have four walls. To enhance the accuracy of the model, it would be beneficial to incorporate the superposition of the impacts of all surrounding walls.

Multiple sensors. The current work focuses on a single pair of transceivers, but in scenarios involving large spaces or multiple targets, the capabilities of a single pair may be limited. To overcome this limitation, a potential solution is to deploy multiple sensors with suitable topologies based on the insights provided by our model [38], [39]. By considering the optimal placement near walls and strategic positioning for improved coverage, a network of multiple sensors can be judiciously distributed throughout the area of interest to expand the sensing capabilities. Future research can explore the development of appropriate topologies and deployment strategies for multiple sensors, allowing for comprehensive and

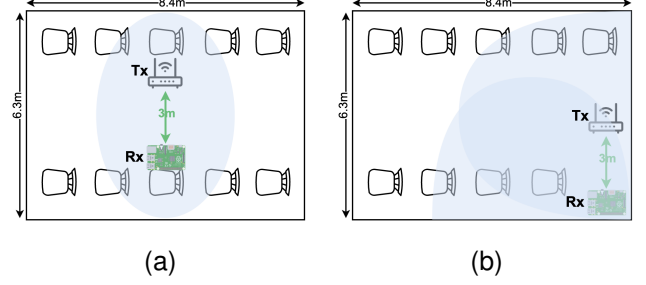


Fig. 22. Enlarging sensing coverage with devices in the same sides. (a) Benchmark. (b) Wall-proximity topology.

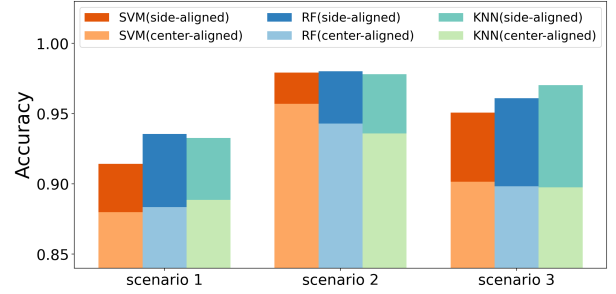


Fig. 23. Comparison of the counting accuracy under double-wall-proximity topologies and benchmarks in various scenarios.

accurate sensing coverage in scenarios where a single pair of transceivers may not be sufficient.

Other factors for optimal device deployment. In the context of stationary crowd counting in this work, the targets were randomly positioned throughout the entire space, without considering the impact of target positions on sensing capabilities. It is crucial to acknowledge that in real-world scenarios, achieving the highest performance may not always involve deploying the devices near the walls. Other factors, such as the positions of the targets, should be taken into account when designing the optimal deployment strategy [31]. By considering the positions of the targets, we can gain a more comprehensive understanding of the effect of device placement on sensing performance. Although our work has made progress in understanding the influence of device placement on sensing, there is still room for further exploration and refinement to better align with real-world scenarios. Incorporating target positions and other relevant factors will contribute to a more accurate and practical understanding of device deployment for sensing applications.

VIII. CONCLUSION

Our work highlights the significant impact of both the wall-device distance and transmitter-receiver distance on Wi-Fi sensing coverage in indoor environments. By introducing a theoretical model, we have successfully demonstrated the relationship between wall-device distances and sensing coverage. The robustness of our proposed model was assessed through the execution of experiments focusing on respiration monitoring and stationary crowd counting across diverse environmental settings. The insights gained from this model enable us to

strategically plan device placement, ultimately expanding the sensing coverage in practical deployments of wall-reflection sensing systems. This research successfully bridges the gap between theoretical understanding and practical implementation, paving the way for improved real-world deployment of such systems. Our findings contribute to advancing the field of Wi-Fi sensing and offer valuable guidance for optimizing sensing performance in indoor environments.

REFERENCES

- [1] Z. Yang, Z. Zhou, and Y. Liu, "From rssi to csi: Indoor localization via channel response," *ACM Computing Surveys (CSUR)*, vol. 46, no. 2, pp. 1–32, 2013.
- [2] Y. Ma, G. Zhou, and S. Wang, "Wifi sensing with channel state information: A survey," *ACM Computing Surveys (CSUR)*, vol. 52, no. 3, pp. 1–36, 2019.
- [3] M. K. A. Jannat, M. S. Islam, S.-H. Yang, and H. Liu, "Efficient wi-fi-based human activity recognition using adaptive antenna elimination," *IEEE Access*, vol. 11, pp. 105 440–105 454, 2023.
- [4] I. A. Showmik, T. F. Sanam, and H. Imtiaz, "Human activity recognition from wi-fi csi data using principal component-based wavelet cnn," *Digital Signal Processing*, vol. 138, p. 104056, 2023.
- [5] X. Zhang, Y. Gu, H. Yan, Y. Wang, M. Dong, K. Ota, F. Ren, and Y. Ji, "Wital: A cots wifi devices based vital signs monitoring system using nlos sensing model," *IEEE Transactions on Human-Machine Systems*, 2023.
- [6] A. Alzaabi, T. Arslan, and N. Polydorides, "Non-contact wi-fi sensing of respiration rate for older adults in care: A validity and repeatability study," *IEEE Access*, 2024.
- [7] D. Khan and I. W.-H. Ho, "Crosscount: Efficient device-free crowd counting by leveraging transfer learning," *IEEE Internet of Things Journal*, vol. 10, no. 5, pp. 4049–4058, 2023.
- [8] H. Jiang, S. Chen, Z. Xiao, J. Hu, J. Liu, and S. Dustdar, "Pa-count: Passenger counting in vehicles using wi-fi signals," *IEEE Transactions on Mobile Computing*, vol. 23, no. 4, pp. 2684–2697, 2024.
- [9] E. Gönültaş, E. Lei, J. Langerman, H. Huang, and C. Studer, "Csi-based multi-antenna and multi-point indoor positioning using probability fusion," *IEEE Transactions on Wireless Communications*, vol. 21, no. 4, pp. 2162–2176, 2021.
- [10] J. Guo, I. W.-H. Ho, Y. Hou, and Z. Li, "Fedpos: A federated transfer learning framework for csi-based wi-fi indoor positioning," *IEEE Systems Journal*, vol. 17, no. 3, pp. 4579–4590, 2023.
- [11] D. Zhang, D. Wu, K. Niu, X. Wang, F. Zhang, J. Yao, D. Jiang, and F. Qin, "Practical issues and challenges in csi-based integrated sensing and communication," in *2022 IEEE International Conference on Communications Workshops (ICC Workshops)*. IEEE, 2022, pp. 836–841.
- [12] C. Chen, G. Zhou, and Y. Lin, "Cross-domain wifi sensing with channel state information: A survey," *ACM Computing Surveys*, vol. 55, no. 11, pp. 1–37, 2023.
- [13] Y. Zeng, D. Wu, J. Xiong, E. Yi, R. Gao, and D. Zhang, "Farsense: Pushing the range limit of wifi-based respiration sensing with csi ratio of two antennas," *Proceedings of the ACM on Interactive, Mobile, Wearable and Ubiquitous Technologies*, vol. 3, no. 3, pp. 1–26, 2019.
- [14] Z. Gao, Y. Gao, S. Wang, D. Li, and Y. Xu, "Crisloc: Reconstructable csi fingerprinting for indoor smartphone localization," *IEEE Internet of Things Journal*, vol. 8, no. 5, pp. 3422–3437, 2020.
- [15] Y. Li, D. Wu, J. Zhang, X. Xu, Y. Xie, T. Gu, and D. Zhang, "Diversense: Maximizing wi-fi sensing range leveraging signal diversity," *Proceedings of the ACM on Interactive, Mobile, Wearable and Ubiquitous Technologies*, vol. 6, no. 2, pp. 1–28, 2022.
- [16] Z. Sun, S. Yan, X. Zhang, and M. Peng, "Modeling and quantitative analysis of motion detection in csi-based sensing," *IEEE Communications Letters*, vol. 26, no. 11, pp. 2809–2813, 2022.
- [17] X. Wang, K. Niu, J. Xiong, B. Qian, Z. Yao, T. Lou, and D. Zhang, "Placement matters: Understanding the effects of device placement for wifi sensing," *Proceedings of the ACM on Interactive, Mobile, Wearable and Ubiquitous Technologies*, vol. 6, no. 1, pp. 1–25, 2022.
- [18] B. Xie, M. Cui, D. Ganesan, and J. Xiong, "Wall matters: Rethinking the effect of wall for wireless sensing," *Proceedings of the ACM on Interactive, Mobile, Wearable and Ubiquitous Technologies*, vol. 7, no. 4, pp. 1–22, 2024.
- [19] Q. Yang, S. He, and J. Chen, "Energy-efficient area coverage in bistatic radar sensor networks," in *2013 IEEE Global Communications Conference (GLOBECOM)*. IEEE, 2013, pp. 280–285.
- [20] T. Xin, B. Guo, Z. Wang, P. Wang, J. C. K. Lam, V. Li, and Z. Yu, "Freesense: A robust approach for indoor human detection using wi-fi signals," *Proceedings of the ACM on Interactive, Mobile, Wearable and Ubiquitous Technologies*, vol. 2, no. 3, pp. 1–23, 2018.
- [21] H. Zhang, Z. Wang, Z. Sun, W. Song, Z. Ren, Z. Yu, and B. Guo, "Understanding the mechanism of through-wall wireless sensing: A model-based perspective," *Proceedings of the ACM on Interactive, Mobile, Wearable and Ubiquitous Technologies*, vol. 6, no. 4, pp. 1–28, 2023.
- [22] T. Woodford, X. Zhang, E. Chai, and K. Sundaresan, "Mosaic: leveraging diverse reflector geometries for omnidirectional around-corner automotive radar," in *Proceedings of the 20th Annual International Conference on Mobile Systems, Applications and Services*, 2022, pp. 155–167.
- [23] D. Tse and P. Viswanath, *Fundamentals of wireless communication*. Cambridge university press, 2005.
- [24] W. Wang, A. X. Liu, M. Shahzad, K. Ling, and S. Lu, "Understanding and modeling of wifi signal based human activity recognition," in *Proceedings of the 21st annual international conference on mobile computing and networking*, 2015, pp. 65–76.
- [25] H. T. Friis, "A note on a simple transmission formula," *Proceedings of the IRE*, vol. 34, no. 5, pp. 254–256, 1946.
- [26] A. Kamann, P. Held, F. Perras, P. Zaumseil, T. Brandmeier, and U. T. Schwarz, "Automotive radar multipath propagation in uncertain environments," in *2018 21st International Conference on Intelligent Transportation Systems (ITSC)*. IEEE, 2018, pp. 859–864.
- [27] M. Dunna, C. Zhang, D. Sievenpiper, and D. Bharadia, "Scattermimo: Enabling virtual mimo with smart surfaces," in *Proceedings of the 26th Annual International Conference on Mobile Computing and Networking*, 2020, pp. 1–14.
- [28] Z. Peng, L. Li, M. Wang, Z. Zhang, Q. Liu, Y. Liu, and R. Liu, "An effective coverage scheme with passive-reflectors for urban millimeter-wave communication," *IEEE Antennas and Wireless Propagation Letters*, vol. 15, pp. 398–401, 2015.
- [29] H. Leaderman and L. Turner, "Theory of the reflection and transmission of electromagnetic waves by dielectric materials," 1948.
- [30] O. Landron, M. J. Feuerstein, and T. S. Rappaport, "A comparison of theoretical and empirical reflection coefficients for typical exterior wall surfaces in a mobile radio environment," *IEEE Transactions on Antennas and Propagation*, vol. 44, no. 3, pp. 341–351, 1996.
- [31] H. Wang, D. Zhang, J. Ma, Y. Wang, Y. Wang, D. Wu, T. Gu, and B. Xie, "Human respiration detection with commodity wifi devices: Do user location and body orientation matter?" in *Proceedings of the 2016 ACM international joint conference on pervasive and ubiquitous computing*, 2016, pp. 25–36.
- [32] T. Koppel, A. Shishkin, H. Haldre, N. Toropovs, I. Vilcane, and P. Tint, "Reflection and transmission properties of common construction materials at 2.4 ghz frequency," *Energy Procedia*, vol. 113, pp. 158–165, 2017.
- [33] F. Gringoli, M. Schulz, J. Link, and M. Hollick, "Free your csi: A channel state information extraction platform for modern wi-fi chipsets," in *Proceedings of the 13th International Workshop on Wireless Network Testbeds, Experimental Evaluation & Characterization*, 2019, pp. 21–28.
- [34] R. K. Pearson, Y. Neuvo, J. Astola, and M. Gabbouj, "Generalized hampel filters," *EURASIP Journal on Advances in Signal Processing*, vol. 2016, pp. 1–18, 2016.
- [35] R. W. Schafer, "What is a savitzky-golay filter?[lecture notes]," *IEEE Signal processing magazine*, vol. 28, no. 4, pp. 111–117, 2011.
- [36] C. J. Willmott and K. Matsuura, "Advantages of the mean absolute error (mae) over the root mean square error (rmse) in assessing average model performance," *Climate research*, vol. 30, no. 1, pp. 79–82, 2005.
- [37] H. Wang and I. W.-H. Ho, "Csi-based passenger counting on public transport vehicles with multiple transceivers," in *2024 IEEE Wireless Communications and Networking Conference (WCNC)*, 2024, pp. 1–6.
- [38] F. Wang, W. Gong, and J. Liu, "On spatial diversity in wifi-based human activity recognition: A deep learning-based approach," *IEEE Internet of Things Journal*, vol. 6, no. 2, pp. 2035–2047, 2018.
- [39] W. Ge, Y. Tian, X. Liu, X. Tong, W. Qu, Z. Zhong, and H. Chen, "Crosstrack: Device-free cross-link tracking with commodity wi-fi," *IEEE Internet of Things Journal*, vol. 10, no. 20, pp. 18028–18041, 2023.